Sultana Rahman, Muhammad Ajmal* and Muhammad Siddiq*

Micron sized anionic poly (methacrylic acid) microgel particles for the adsorptive elimination of cationic water pollutants

https://doi.org/10.1515/zpch-2022-0147
Received October 21, 2022; accepted December 14, 2022; published online January 2, 2023

Abstract: In this article, we reported the micron sized particles of poly (methacrylic acid) (p [MAA]) microgel and explored their applications as anionic adsorbents. The micron sized particles of poly (methacrylic acid) microgel were prepared by a simple inverse suspension polymerization method. The adsorptive elimination of adsorbates of cationic nature including malachite green (MG) and methylene blue (MB) from the aqueous medium was studied systematically. The adsorption tests were carried out using various initial concentrations of dyes and with different amounts of adsorbents. The adsorption equilibrium was established in 60 min. The adsorption capacity of the p (MAA) microgel was found as high as 351 mg/g for MG and 65 mg/g for MB. The maximum removal percentage for MG and MB was recorded as 88 and 68%, respectively. The adsorption data was computed with adsorption isotherm models including Langmuir, Freundlich, and Temkin. The Langmuir model was observed to be more applicable for the adsorption of MG while the adsorption of MB was best matched with Temkin model. The adsorption data was also treated with pseudo first order and pseudo second order kinetic models along with intraparticle diffusion and Elovich models. The pseudo second order kinetic model was most suitable with adsorption of both the MG and MB.

Keywords: adsorption; adsorption capacity; cationic pollutant; methacrylic acid; microgel.

1 Introduction

Water is the most important ingredient for all the living organisms on our planet, but unfortunately it is contaminated by many industries and become unsafe for

***Corresponding authors: Muhammad Ajmal**, Department of Chemistry, Division of Science and Technology, University of Education, Lahore, Pakistan, E-mail: m.ajmal65@yahoo.com; and
Muhammad Siddiq, Department of Chemistry, Quaid-i-Azam University, Islamabad 45320, Pakistan, E-mail: m_sidiq12@yahoo.com
Sultana Rahman, Department of Chemistry, Quaid-i-Azam University, Islamabad 45320, Pakistan

ecosystem. Due to high industrialization and their increasing effluents, water contamination is at its highest rate ever. The effluents of the primary pollutants that poison water are those liberated from the textile and other coloring industries that threaten both marine and human life [1, 2]. Along with many other water pollutants, synthetic dyes found in the clothing and food sectors are considered as life-threatening water contamination because of their inability to decompose naturally, highly toxic for sea species, and harmful impacts on people [3, 4]. Synthetic dyes are a broad category of organic chemicals that can be found in almost every aspect of our daily lives. Hazardous azo dyes of different sorts have been discovered in the waste products of several sectors comprising printing, plastics, latex, pulp, leather, and fabric etc. [5]. The azo dyes elimination is a huge concern because of these dyes as well as their degradation products are the reason of serious health problems and harm the environment. The azo dyes malachite green (MG) and methylene blue (MB) are among the most commonly used dangerous azo dyes in numerous industries, though they can metabolize to the harmful intermediate benzidine, which is a human carcinogen [6]. The toxicity of MG and MB have been known for many years. Foster and Woodbury et al. have earlier reported the usage of MG as a potent antibacterial and fungicide in fisheries in 1936, for the purpose of treating marine fish infections, allowing the transport of marine products, and disinfecting water tanks [7]. Stammati et al. in 2005 reported that once MG penetrates into marine species, it transforms into a fat-soluble component and bioaccumulates, posing a risk of poisoning to humans through the food chain [8]. Food safety has become a significant worldwide challenge as a result of social advancement and the rising diversity of food products that are readily available worldwide [9]. Fallah and Barani et al. reported in their research in 2014 that in fatty fish and tissues the malachite green and their compounds are digested very slowly [10]. The toxicity of MG for fish has been reported quantitively by Omoregie et al. and they found 85.1% mortality of *O. niloticus* at MG concentration of 1.20 ppm in water [11]. Similarly, 20 times increase in the mortality rate of eggs and fries largemouth bass, Micropterus salmonids was reported by Wright [12]. The acute toxicity of MG for fish was reviewed by Srivastava et al. in terms of its LC50 (amount suspended in the air required to kill 50% of a test animals in a predetermined observation period) value and found it as low as 0.0453 ppm for *Micropterus dolomieui* [13]. Moreover, the usage of MG pollutes water resources because of the sluggish metabolism and degradation of MG in the surroundings [14]. Due to above mentioned results, international government units described MG and MB as poisonous, damaging, harmful, polluting and corrosive. MB has therapeutical use in the treatment of acquired and idiopathic methemoglobinemia, but MB tolerance varies considerably in the different animal species. Quantitatively, it has been found that upon exposure to MB concentration of 200 mg/kg, 70% of treated rabbits developed Heinz bodies within 96 h of treatment

[15]. Despite of their acute toxicity, MG and MB are used in many industrial processes unavoidably. These dyes of numerous qualities are used in massive amounts to color jute, cotton, paper, wool and leather etc. [16, 17]. Mostly terrifying, 10–15% of cationic dyes including MG and MB are directly lost to wastewater in these methods [18]. In this scenario, finding an effective treatment method to remove these hazardous dyes from industrial effluents is crucial. The colored effluents or wastewater must be treated adequately before being discharged into aquatic sources [19, 20]. For the handling of dye-comprising wastewater, a variety of processes have been used, including adsorption [21], biological degradation using bacteria [22], heterogeneous photocatalysis [23], membrane filtration, electrocoagulation, chemical precipitation, reverse osmosis, photocatalytic degradation, decantation, and flocculation [24]. Among the above stated, adsorption has been identified as a truly desirable technique of separation for the secure and fast elimination of dyes from wastewater. Therefore, research is being focused on finding and/or designing cost-effective and efficient adsorbents [25]. Many adsorbents, including carbon nanotubes [26], multi wall carbon nanotubes (MWCNTs) [27], activated carbon [28], fly ash [29], chitin [30], zeolite [31], polymers [25], lignin [32], barley straw [33], nanocomposites [34], and graphene oxide [35], have been examined for the hazardous dyes elimination. Three dimensional polymeric networks with hydrophilic groups, known as hydrogels, have gained scientific interest in recent decades due to their high adsorption capacity. Polymeric hydrogel adsorbents exhibit high adsorption potential due to their porous structure [36] and have been known to be the most promising adsorbents for the inorganic pollutants elimination (like heavy metals), and organic pollutant (like phenolic compounds, dyes and pesticides) from waste water and some ions from aquatic sources, for example phosphate [37], nitrate [38], and harmful heavy metals [39]. The natural polymer hydrogels have been found as biodegradable, relatively cost effective, non-toxic and eco-friendly adsorbents [40]. However, synthetic polymer hydrogels have shown tremendous adsorption potential as they can be designed with on-demand chemical composition. For example, Hemant et al. designed a polyacrylamide based hydrogel and found it to possess extensive potential for decontamination of industrialized sewerage poisoned by toxic azo dyes [41]. Similarly, organic/inorganic hydrogel nanocomposite of titania combined with sodium alginate crosslinked poly (acrylic acid) (SA-cl-poly [AA]-TiO_2) was reported by Thakur et al. for the effective MB elimination by batch adsorption process from water. Cheng et al. prepared graphene oxide (GO) based magnetic composite hydrogels by integrating GO with poly (vinyl alcohol) and platinum (Pt) nanoparticles and investigated their adsorptive application. The researchers concluded that such hybrid hydrogels have a significant property of adsorption for the removal of water pollutants [42]. The adsorptive removal of copper (II) and cobalt (II) ions was studied by Naseem et al. with an anionic smart polymer microgel and found that electrostatic interaction

between anionic microgel and cationic pollutants becomes helpful to enhance the efficiency of the adsorbent [43]. A tow fold environmental application of microgels was reported by shahid et al. by extracting the cobalt (II) ions from water by sorption followed by their conversion into catalytically active nanoparticles by *in situ* reduction [44]. This work demonstrated that microgel cannot be used only as adsorbent to remove a pollutant from aqueous medium, but the same pollutant can be converted into a catalyst; a beneficial product. Similarly, Farooqi et al. designed a microgel which was used to extract silver (I) ions from aqueous medium and converted them into a catalyst having potential to accelerate the reduction of MG [45]. Due to ease of polymerization and control on morphology, MAA based copolymer microgels have gained much attention in drug delivery, controlled synthesis of nanoparticles, catalysis, and adsorption [46]. Despite of the extensive work on hydrogel adsorbents, researchers are exploring the effects of chemical compositions and morphology of the hydrogel to find economical, user friendly and environment friendly adsorbents. In this context, we have contributed p (MAA) hydrogel in the form of micron sized particles as adsorbent to eliminate the cationic water contaminants. MG and MB coloring agents were chosen as representative cationic water contaminants. Optimum amount of adsorbent and time of the adsorption process under the specific conditions were analyzed. Adsorption isotherms and kinetic models were employed to the adsorption results to get insights of the adsorption method.

2 Materials and methods

2.1 Chemicals and reagents

We have used methacrylic acid (MAA, 97%, Alfa Aesar) as a monomer, ammonium persulfate (APS 99%, Sigma Aldrich) as initiator, *N,N*-methylenebisacrylamide (MBA, 98%, Sigma Aldrich) as a cross-linking agent, and *N,N,N,N* – Tetramethylethylenediamine (TEMED, 97%, Merck) as an accelerator. The solvent used during the experiment was cyclohexane (97%). Sorbitan mono laurate span 80 was utilized as surfactant. Sodium hydroxide (NaOH, 99%, Sigma) was applied as a base. As representative cationic adsorbents, we used methylene blue (MB, DC Panreac) and malachite green (MG). This study was carried out with deionized (DI) water.

2.2 Preparation and characterization of poly (methacrylic acid) microgel

The preparation and characterization of poly (methacrylic acid) microgel particles have already been reported in our earlier publication [47].

2.3 Adsorption study

The stock aqueous solutions of MG and MB were prepared and utilized to prepare further solutions of required concentrations by dilution method. To optimize the amount of adsorbent, a 100 ml aqueous solution of MG (60 ppm) and MB (80 ppm) were separately contacted with varying amounts of adsorbents in the range of 0.05–0.15 g and 0.025–0.1 g, respectively. Initial MG and MB concentrations affect the adsorption parameters, and it was examined using solutions with varying initial concentrations of 60, 120, 240, 300, and 360 ppm for MG and 20, 30, 40, 50, 60, 70, 80 ppm for MB. The amount of adsorbent (0.06 mg for MG and 0.01 g for MB) and the volume of MG solution of the dyes (100 mL) were kept constant. The adsorption procedure was carried out at constant stirring speed of 350 revolutions per minute and at room temperature. At different intervals of time, 0.5 mL for MG and 1.0 mL for MB sample were collected from the adsorption medium. The samples were diluted with optimum amounts of DI water before their further examination. The UV–visible spectrophotometer was used in order to measure the amount of MG and MB adsorbed in terms of absorbance at the highest absorption wavelengths (617 nm for MG and 660 nm for MB).

3 Results and discussion

3.1 Morphology of p (MAA) microgel

The detailed discussion on the preparation and characterization of p (MAA) microgel particles have already been reported in our earlier publication [47]. However, a representative SEM image is shown in Figure 1 which shows that spherical shaped, micron sized particle of p (MAA) microgel were prepared and diameters of most of the particles were in the range of 60–95 μm.

3.2 Adsorption studies

MG and MB were chosen as the representative cationic adsorbates to measure the adsorption potential of the synthesized p (MAA) microgel adsorbent. The p (MAA) microgel furnish anionic carboxylate groups. An electrostatic force of attraction is created among the cationic dye molecules and anionic p (MAA) microgels when they come in contact in the aqueous medium. This electrostatic force of attraction becomes the factor that drives the migration of dye molecules from the aqueous solution to the p (MAA) microgel networks. For systematic analysis, the time and amount of adsorbate was optimized for 100 ml aqueous solution of MG (60 ppm) and MB (80 ppm). The amounts of dyes adsorbed on the per unit mass of p (MAA) microgel were calculated by the well-known mass-balance equation (1).

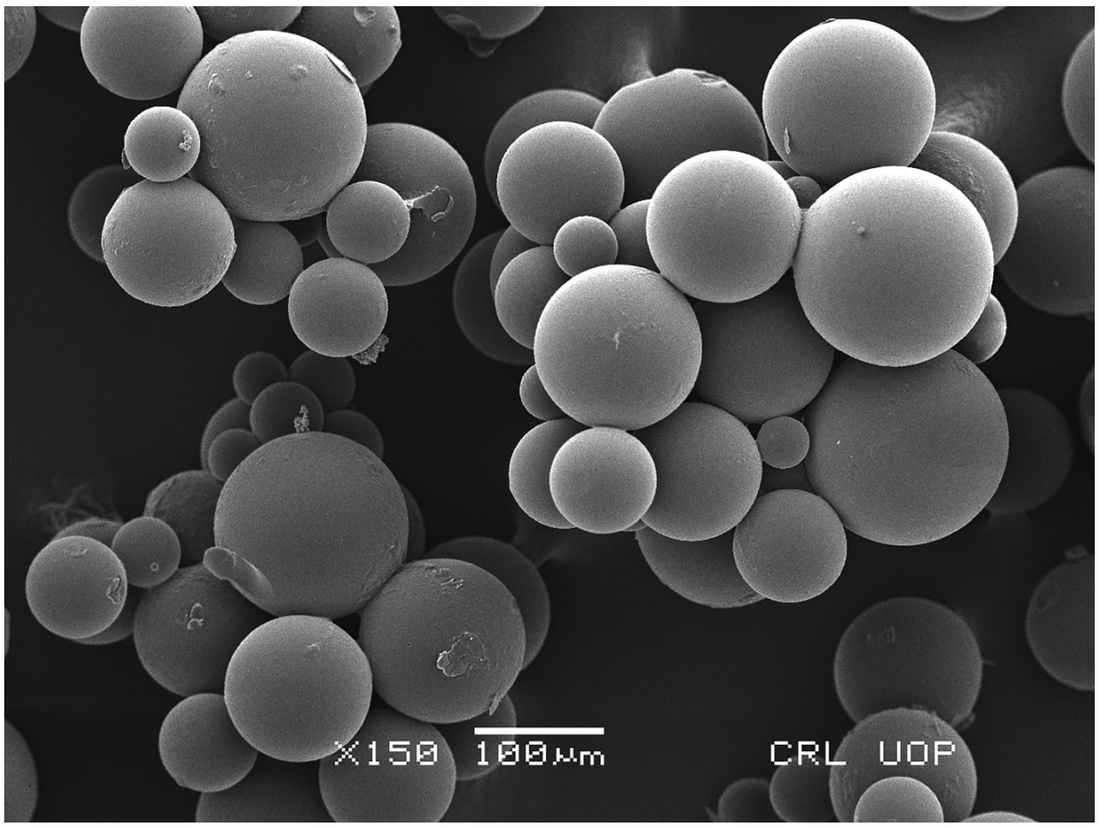

Figure 1: SEM image of p (methacrylic acid) microgel.

$$q = (C_0 - C_t) \times V/m \tag{1}$$

In equation (1), C_0 and C_t represent the initial and time-varying dye solution concentration, V refers to initial volume of dye's solution, and the m stands for dried mass of the p (MAA) microgel used as adsorbent.

Figure 2(a) and (b) shows the % removal of MG and MB in relation to the time. The observations revealed that % removal was increased as the adsorbent amount was raised. This observation of increase in % removal with the increasing quantity of adsorbent is due to the rise in adsorption surfaces in the medium. Almost 68% of MG from its 60 ppm, 100 ml solution was adsorbed on the 0.15 g of p (MAA) microgel with a corresponding equilibrium time of 60 min as depicted from Figure 2(a). On the other hand, 88% removal of MB was recorded from its 80 ppm, 100 ml solution upon contacting with 0.05 g or higher amount of p (MAA) microgel with a corresponding equilibrium time of 60 min as depicted from Figure 2(b). Figure 2(a) and (b) also demonstrates that the initial straight portions of the graphical lines were shifted towards *y*-axis with higher values of slopes and indicated an increase in the rate of adsorption. This observation is associated to increase in the available adsorption sites per unit volume in the adsorption medium.

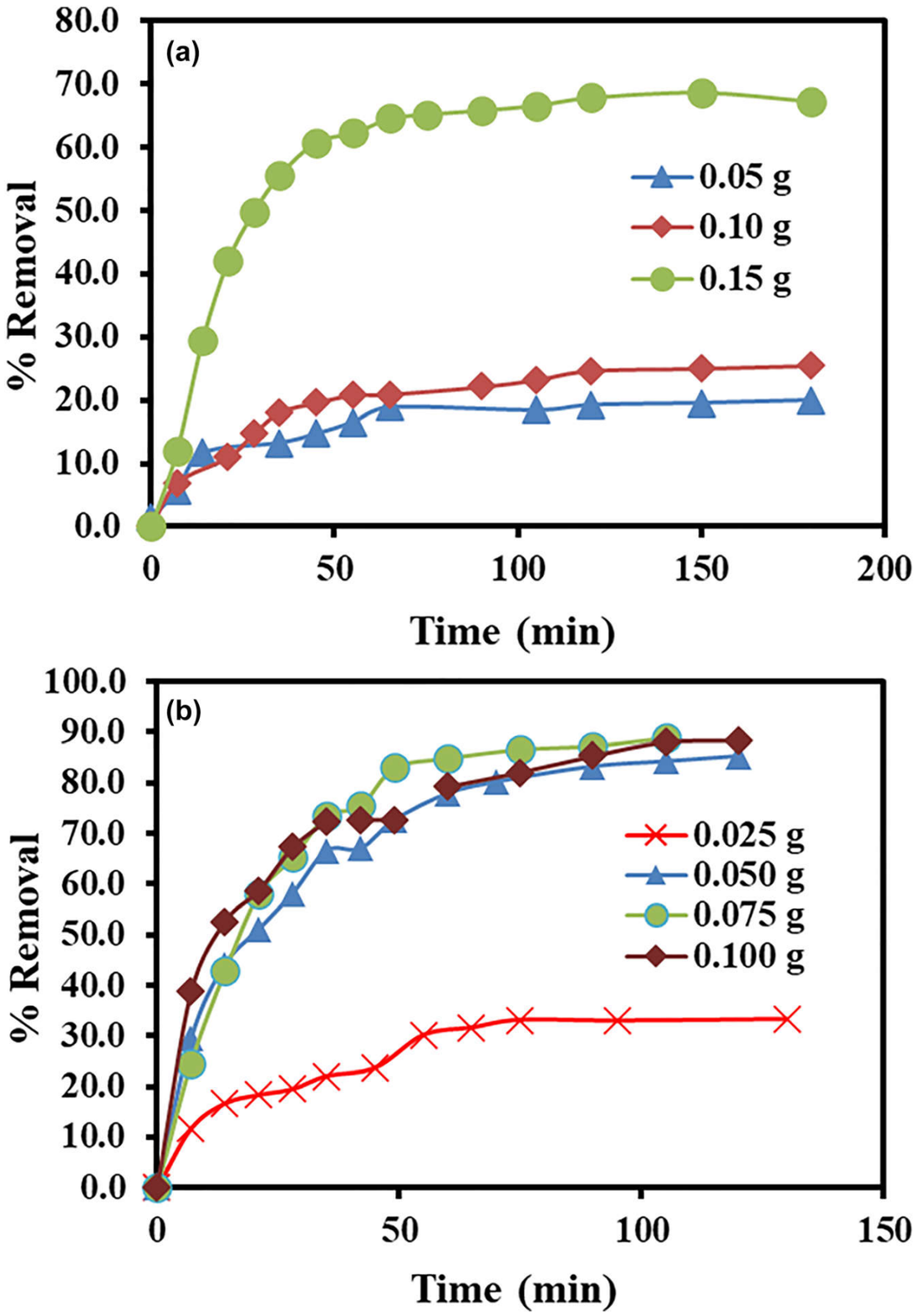

Figure 2: Plots of % removal for malachite green and (b) methylene blue in relation to time with varying p (MAA) microgel quantities [100 ml solution of 60 ppm MG and 80 ppm MB, room temperature].

The adsorbate's initial concentration also effects the process of adsorption. Therefore, sorption equilibrium and kinetics were also studied at various initial concentrations of dyes aqueous solutions. Figure 3(a) shows the MG amount adsorbed from each various initial concentration solution. As it is depicted from Figure 3(a), by rising the concentration of MG from 60 to 360 ppm, the extent of adsorption was also increased from 50 to 351 mg/g. Related findings were also examined for MB and the extent of adsorption was raised from 5 to 65 mg/g corresponding to a rise in the MB initial concentration from 20 to 80 ppm as indicated in Figure 3(b). The rise in the extent of adsorption upon increasing the adsorbate's solution initial concentration can be explained in a way that with low initial concentration of adsorbate solution, the adsorption active sites remain unoccupied and upon increasing the initial concentration, the adsorption sites are gradually occupied and hence the extent of adsorption was increased.

3.3 Adsorption isotherms

The optimum relationship between the mass of adsorbate which accumulates on the adsorbent and the adsorbate solution concentration when the constant temperature kept throughout the process is characterized as an adsorption isotherm [48]. Adsorption isotherms are utilized to examine the relationship of adsorbate with the adsorbent surface. The adsorption isotherms are employed to find out the adsorption nature using the results of impact of initial concentration of the adsorbate in solution. At a steady temperature, the adsorption investigation is carried out. The suitable adsorption isotherm model shows a vital part in validating the adsorption process of the adsorbent-adsorbate system [49, 50]. Numerous adsorption isotherms have been established to report the impacts of various factors on adsorption capacity, rate of adsorption, and equilibrium state. Langmuir, Freundlich and Temkin adsorption isotherms are the more frequent to notice the adsorption phenomenon. The Langmuir adsorption isotherm model implies monolayer adsorption at a specific or limited number of similar localized spots, with low lateral contact and steric barrier among species of the adsorbate and even on adjacent locations. Additionally, throughout the adsorption process, this model relates to homogenous adsorption, where each site has a same quantity of energy [51, 52]. The Langmuir isotherm neglects surface roughness of the adsorbent, non-identical adsorption sites, and the creation of adsorbate molecules multilayer on the adsorbent sites. However, the presence of these characteristics was not overlooked in Freundlich adsorption isotherm. Adsorption characteristics may be influenced by interactions between adsorbate molecules and adsorbent sites. The Temkin adsorption isotherm takes this interaction into account, it claims that as the number of molecules of adsorbate

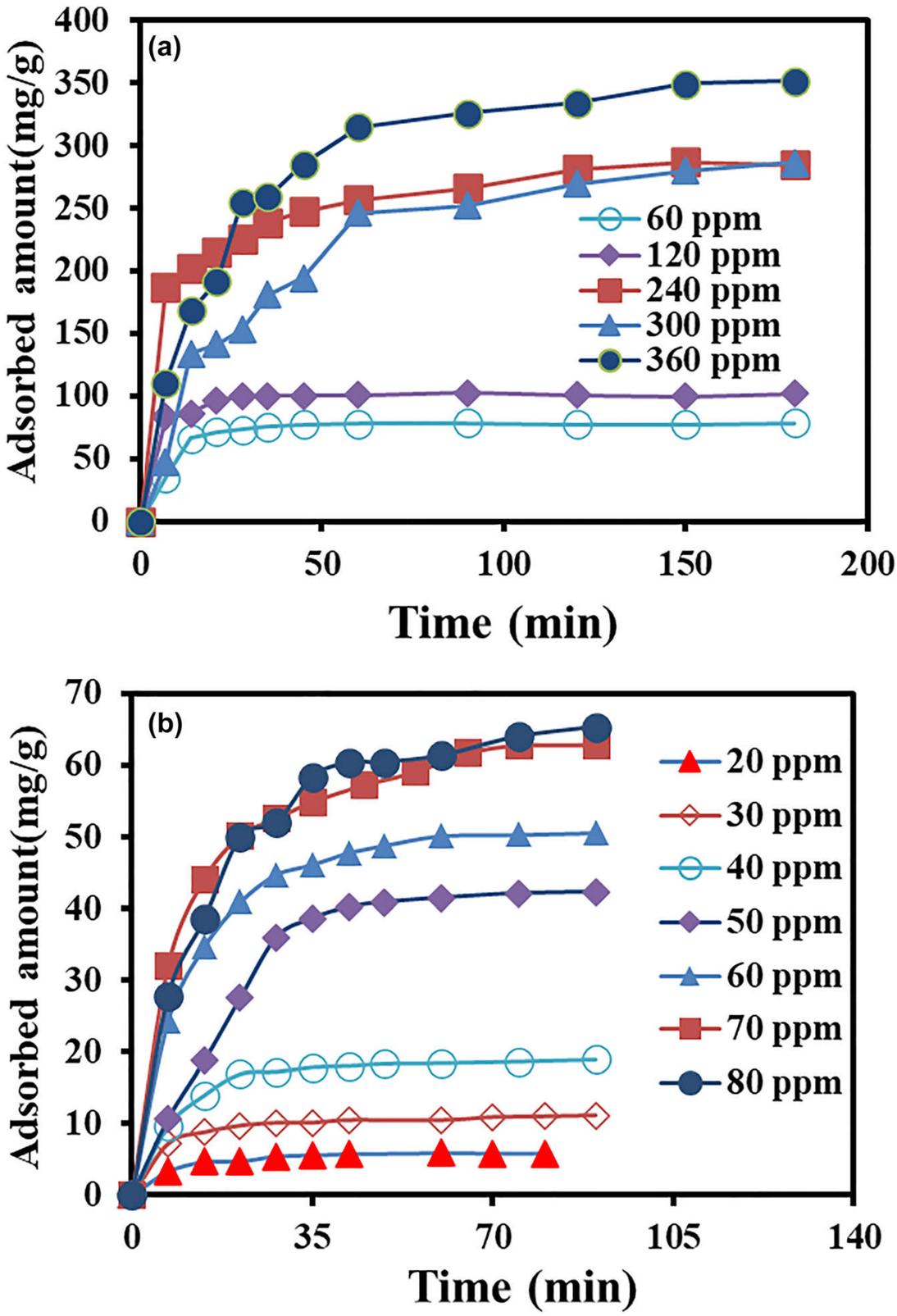

Figure 3: Quantity of (a) Malachite Green and (b) Methylene Blue adsorbed on p (MAA) microgel from their solutions of different concentrations (100 ml of adsorbate solution, p (MAA) adsorbent = 0.06 g for MG and 0.1 g for MB, Room temperature).

adsorbed on the adsorbent increases, the heat of adsorption of all molecules in the adsorption layer decreases sharply, indicating a potential two-way association in between adsorbate and adsorbent. The linear mathematical expressions of Langmuir, Freundlich and Temkin are specified by Equation (2)–(4) respectively.

$$C_e/q_e = C_e/q_m + 1/q_m K_L \tag{2}$$

$$\ln q_e = \ln K_F + 1/n \ln C_e \tag{3}$$

$$q_e = B \ln K_T + B \ln C_e \tag{4}$$

Here, C_e is the MG and MB equilibrium concentration solution, and q_e is the MG and MB quantity adsorbed per gram of p (MAA) adsorbent at equilibrium. The term q_m denotes the maximum adsorption capacity of p (MAA) for MG and MB, and K_L denotes the Langmuir adsorption constant. Figure 4(a) and (b) provide the graphical illustration of the Langmuir adsorption isotherm for MG and MB, respectively. The coefficient of determination (R^2), q_m, and K_L values were determined by the graphs and depicted in Table 1. The R^2 was found 0.9968 for MG. The value of q_m was estimated from the Langmuir isotherm slope and noticed as 400 mg/g for MG which was closest to its experimental value 352 mg/g. These observations reveals that the adsorption of MG was accompanied by Langmuir model and the surface of p (MAA) microgel was uniform throughout with equivalent adsorption sites. On the other hand, R^2 for Langmuir isotherm of MB was determined to be 0.8865 which is far from 1. Also, the value of q_m was found to be –11.534 mg/g. This negative value of q_m ruled out the fitting of Langmuir isotherm on the adsorption of MB.

Figure 5(a) and (b) represents the plot of Freundlich adsorption isotherm of MG and MB, respectively. The corresponding parameters were calculated and presented in Table 1. In the Freundlich isotherm, the parameter n is very important. The $1/n$ ratio reveals the bond nature between the adsorbent and adsorbate. Chemisorption is represented by a value of $1/n$ from 0 to 1. Moreover, $1/n$ value in between 0.7 and 1 indicates that raising the adsorbate solution concentration reduces the absolute adsorption. This occurs because the saturation of the available adsorption sites. Furthermore, the significance of $1/n$ shows the degree of heterogeneity on the surface of adsorbent. A $1/n$ value from 0 to 1 suggests chemisorption and the existence of heterogeneity on the adsorbent sites, and the nearer ratio of $1/n$ is to 0, the more heterogeneity is there on the adsorbent surface [53]. The value of $1/n$ in this study was 0.4470, 0.1950 for MG and MB, respectively, as given in Table 1 and indicated that the chemisorption was the process occurred. This $1/n$ number was very nearer to zero when compared to 1, implying that the adsorbent surface was having some degree of heterogeneity. However, the values of R^2 of Freundlich adsorption isotherm of MG

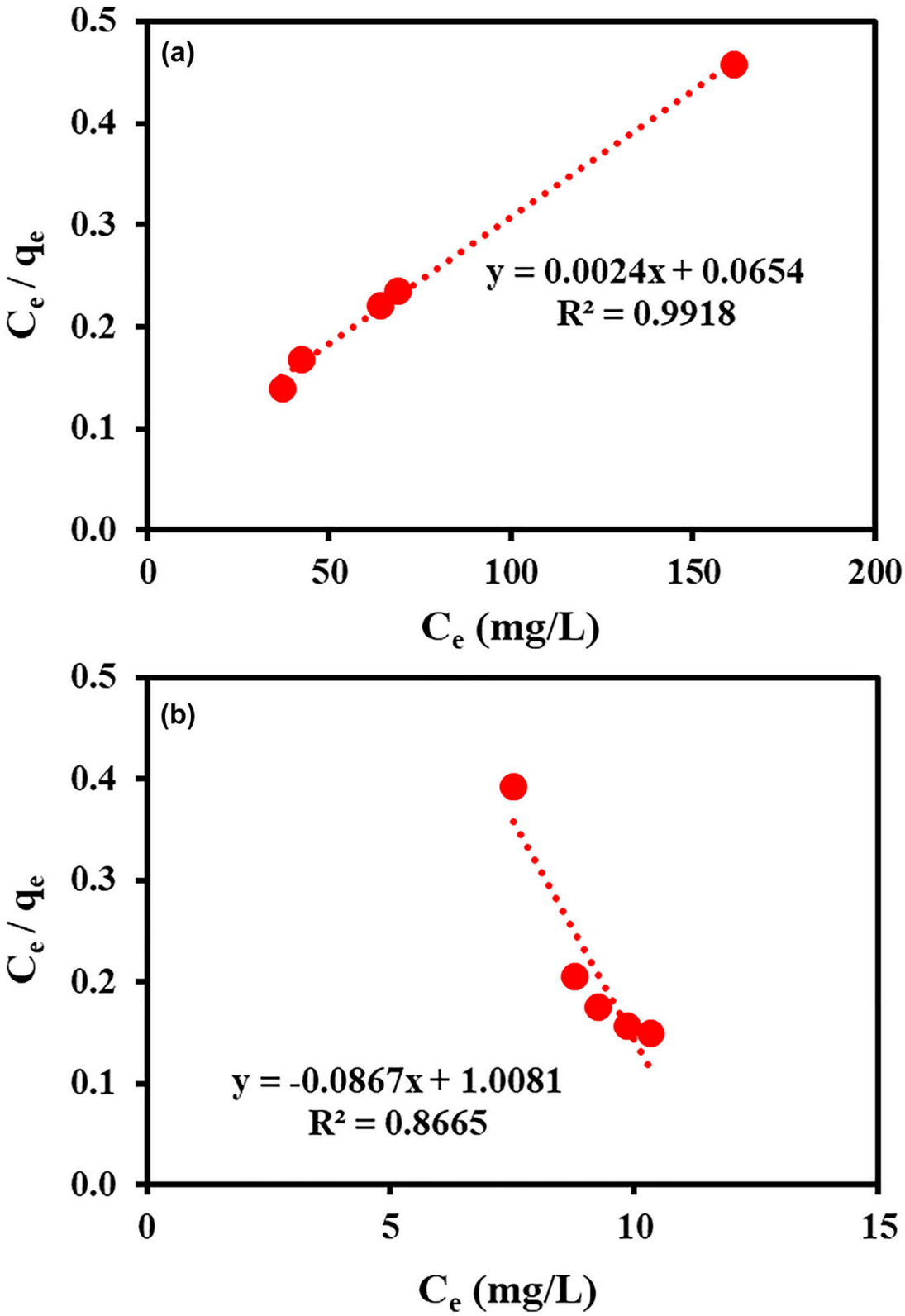

Figure 4: Application of Langmuir isotherm for the adsorption of (a) malachite green and (b) methylene blue onto the p (MAA) microgel (Conditions of reaction; solution of MG [60–360 ppm] = 100 ml, p (MAA) microgel = 0.06 g, MB solution [20–80 ppm] = 100 ml, p (MAA) microgel = 0.1 g, room temperature).

Table 1: The calculated parameters and determination coefficients values of the adsorption isotherms for MG and MB are summarized (Reaction conditions; MG solution [60–360 ppm] = 100 ml, MB solution [20–80 ppm] = 100 ml, p (MAA) microgel = 0.06 g for MG, and 0.1 g for MB, room temperature).

Dye	Langmuir isotherm constants			Freundlich isotherm constants			Temkin isotherm constants		
	K_L (L/g)	q_m (mg/g)	R^2	K_F (L/g)	n	R^2	K_T (L/g)	B	R^2
MG	23.48	351.00	0.996	4572.99	0.447	0.926	1.250×10^4	0.002	0.950
MB	11.44	−11.53	0.886	36,957,279.97	0.195	0.920	1.184×10^4	0.005	0.990

and MB, do not strongly support that our data follows the Freundlich adsorption isotherm.

Figure 6(a) and (b) presents the graphical representation of the Temkin adsorption isotherm generated by displaying q_e with relation to ln C_e. The values of R^2 for MG and MB were 0.9506 and 0.9909, individually. These values are much closer to 1 as compared to those observed in Freundlich isotherms. So, this overall analysis of the isotherms reveals that the MG adsorption was best matched with Langmuir model and that MB was best fitted with Temkin model.

Since a variety of adsorbents with various structures and compositions have been emerged and tested for the adsorptive elimination of MG and MB. So, we have compared our results with those already reported in literature. Table 2 shows various adsorbents and their reported adsorption capacities for MG. This comparison is representing that our reported adsorbent showed significantly better adsorption potential as compared to many previously reported adsorbents.

3.4 Adsorption kinetics

To get insights of the absorption process, the adsorption data was computed with pseudo first-order and pseudo second order, intra particle diffusion and Elovich kinetic models to determine the rate constants and order of reactions for the adsorption processes.

The equations (5) and (6) are representing the linear forms of pseudo first-order and pseudo second-order kinetics expressions, individually.

$$\log(q_e - q_t) = \log q_e - k_1.t/2.303 \tag{5}$$

$$t/q_t = 1/k_2.q_e^2 + t/q_e \tag{6}$$

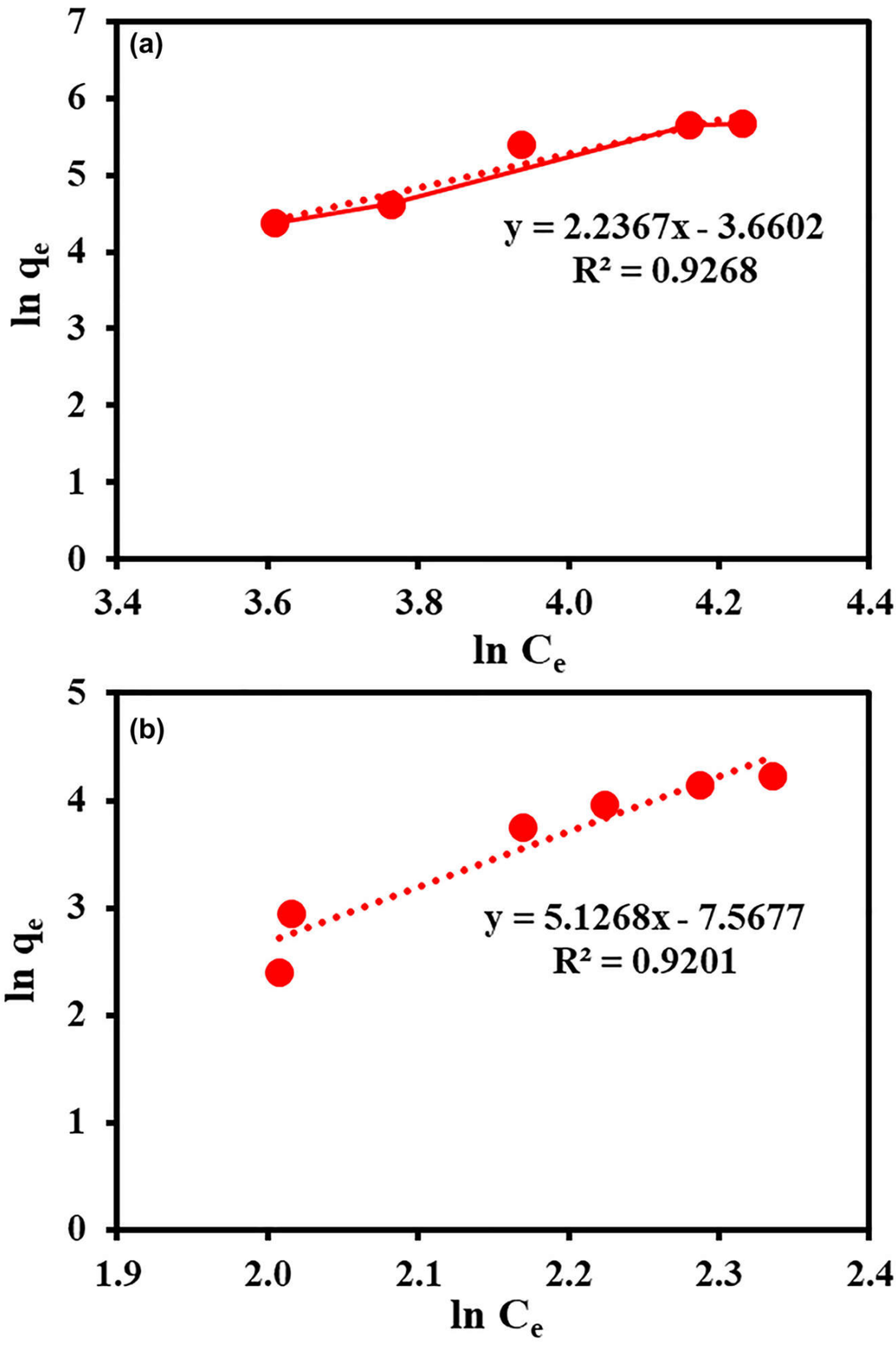

Figure 5: Application of Freundlich adsorption isotherm to the adsorptive elimination of (a) malachite green and (b) methylene blue onto the p (MAA) microgel (Conditions of the reaction; solution of MG [60–360 ppm] = 100 ml, p (MAA) microgel = 0.06 g, MB solution [20–80 ppm] = 100 ml, p (MAA) microgel = 0.1 g, room temperature.).

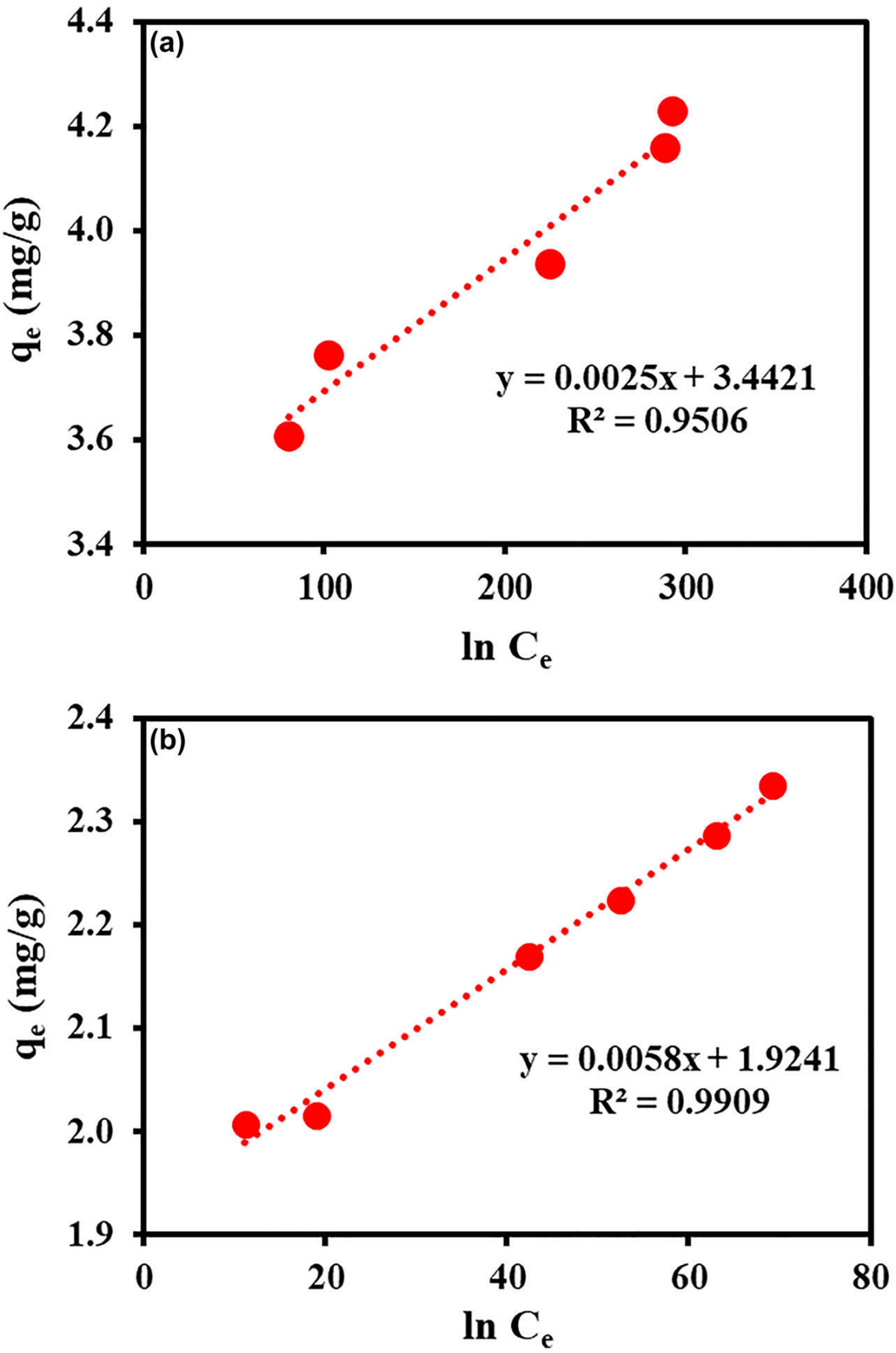

Figure 6: Application of Temkin adsorption isotherm on the adsorptive elimination of (a) malachite green and (b) methylene blue onto the p (MAA) microgel (Reaction conditions; solution of MG [60–360 ppm] = 100 ml, p (MAA) microgel = 0.06 g, MB solution [20–80 ppm] = 100 ml, p (MAA) microgel = 0.1 g, room temperature).

Table 2: The various adsorbents' capacities for adsorption with the adsorption capacity of our currently reported poly (methacrylic acid) microgel for capturing malachite green.

Adsorbent	Adsorption capacity (mg/g)	Reference
Amino-modified SiO_2@ Fe_3O_4 magnetite	173	[54]
MMT clay	262.5	[55]
Starch-g-poly (acrylamide)/GO/hydroxyapatite	297.0	[56]
Poly (acrylic acid-co-acrylamide) hydrogel composite	238.09	[57]
Chitosan/MMT	322.58	[58]
Poly (methacrylic acid) hydrogel	351.774	Present work

Here, q_e and q_t are the milligrams of the adsorbate adsorbed per gram of the adsorbent at equilibrium time (minutes) and at time t (minutes). While k_1 and k_2 are the rate constants for pseudo first-order and pseudo second-order kinetics, respectively. Plot of $\log(q_e - q_t)$ versus time yielded the graphical form of pseudo first-order kinetics for MG and MB as manifested separately in Figure 7(a) and (b). The corresponding parameters were computed from the graphs, and the results are summarized in Table 3. Similarly, graphical form of pseudo second-order kinetics for MG and MB were yielded separately by plotting t/q_t versus of time (t) as shown in Figure 8(a) and (b). The related parameters were computed from the plots and are provided in Table 4 which evidenced that the rate constant, k_2, decreased as the initial dye concertation was increased. Additionally, at all examined doses of MG (60–360 ppm) and MB (20–80 ppm), the computed q_e values were discovered to be near the experimental q_e values. The higher values of R^2 and the close correlation between the values of q_e determined from the pseudo second-order kinetics and the experimental process suggested that the MG and MB adsorption were succeeded by pseudo second-order kinetics model. These outcomes indicate the possibility that the rate-limiting stage of the adsorption process may be intrinsic chemisorption rather than diffusion as assumptions of pseudo first-order kinetics.

Since p (MAA) microgel has porous structure due to its crosslinked polymeric network and empty space in the structure, the dyes can be transported into the pores through the interface between the solution and the adsorbent. Therefore, experimental data was also computed with IPD model. The expression (7) represents the linear mathematical equation of IPD model.

$$q_t = k_{id}.t^{0.5} + C \tag{7}$$

Here, k_{id} is the IPD rate constant (mg/g $min^{0.5}$) and C (mg/g) is a constant and presents the value of q_t when k_{id} or t approaches to zero. The graphical forms of linear equation of IPD Model for MG and MB are depicted in diagram 9 (a) and (b),

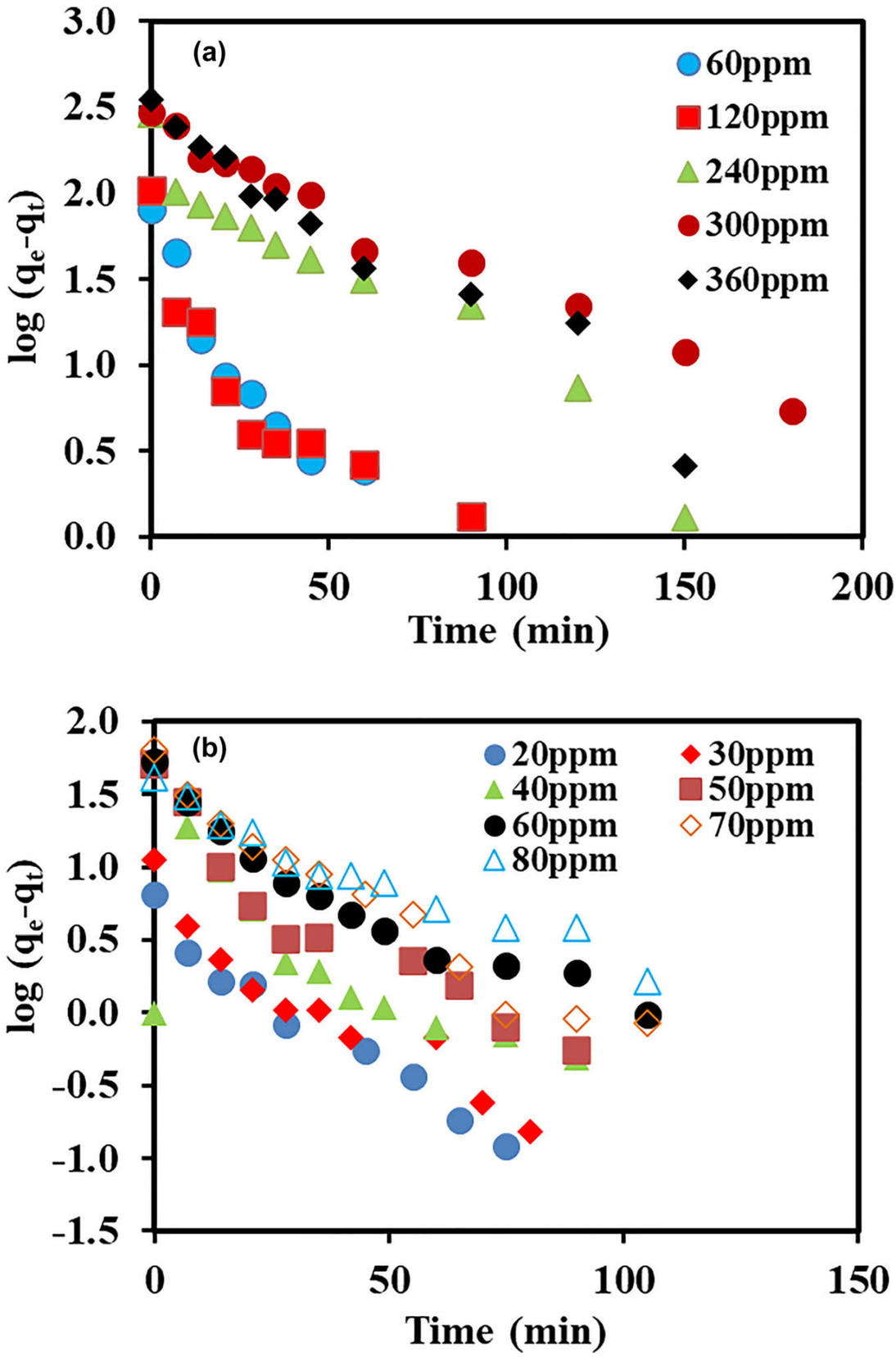

Figure 7: Linear kinetic profiles of pseudo first order for the adsorption of (a) MG and (b) MB from their various initial concentrations (Reaction conditions; 100 ml solution of MG [60–360 ppm], MB [20–80 ppm], p (MAA) adsorbent = 0.06 g for MG and 0.1 g for MB, room temperature).

Table 3: Pseudo first order kinetic parameters calculated from the linear profiles for the adsorption of (a) MG and (b) MB from their various initial concentrations. The values of k_1 and q_e are represented in min^{-1} and mg g^{-1}, respectively (Reaction conditions; 100 ml solution of MG [60–360 ppm], MB [20–80 ppm], p (MAA) adsorbent = 0.06 g for MG and 0.1 g for MB, Room temperature).

Initial concentration	Constants	Malachite green (MG)	Methylene blue (MB)
MG = 60 ppm	k_1	–0.059	–0.047
MB = 20 ppm	q_e (calculated)	46.751	4.312
	q_e (experimental)	80.164	6.508
	R^2	0.777	0.968
MG = 120 ppm	k_1	0.059	–0.044
MB = 30 ppm	q_e (calculated)	48.117	5.989
	q_e (experimental)	103.580	8.151
	R^2	0.963	0.910
MG = 240 ppm	k_1	–0.029	–0.047
MB = 40 ppm	q_e (calculated)	162.032	9.808
	q_e (experimental)	288.403	19.130
	R^2	0.938	0.942
MG = 300 ppm	k_1	–0.022	–0.045
MB = 50 ppm	q_e (calculated)	255.035	23.329
	q_e (experimental)	291.952	42.397
	R^2	0.988	0.896
MG = 360 ppm	k_1	0.029	–0.035
MB = 60 ppm	q_e (calculated)	290.001	27.246
	q_e (experimental)	351.774	52.494
	R^2	0.972	0.917
MB = 70 ppm	k_1	–	–0.046
	q_e (calculated)	–	45.186
	q_e (experimental)	–	63.808
	R^2	–	0.972
MB = 80 ppm	k_1	–	–0.028
	q_e (calculated)	–	36.433
	q_e (experimental)	–	70.255
	R^2	–	0.965

k_1= rate constants for pseudo first-order kinetcs, q_e = amount of adsorbate adsorbed per gram of the adsorbent at equilibrium condition, R^2 = coefficient of determination.

respectively. The corresponding calculated variables are given in Table 5. As demonstrated by the Figure 9(a) and (b), the kinetic profiles can be divided into three linear segments with different slopes. It indicates the presence of non-uniform and irregular pore size and surface of the adsorbent which is obvious in three-dimensional cross-linked structure of p (MAA) microgel. Fast sorption was seen within the first 5 min, and the initial curved zone resembles to the absorption from the external surface. The next phase is related to progressive absorption, with the rate-limiting step being intraparticle diffusion, and the last plain zone denotes

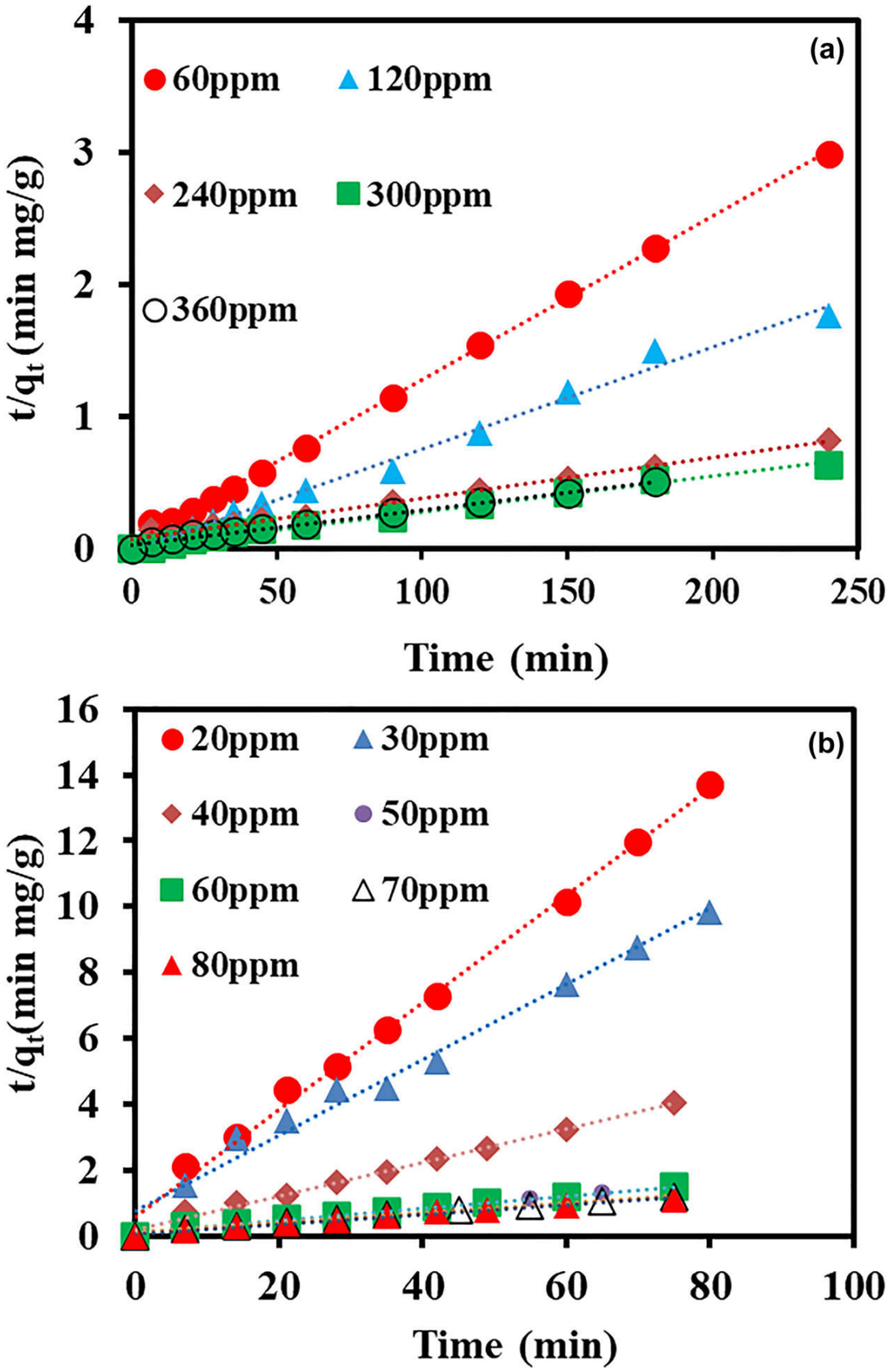

Figure 8: Linear kinetic profiles of second order for the adsorption of (a) MG and (b) MB from their different initial concentrations (Reaction conditions; 100 ml solution of MG [60–360 ppm], MB [20–80 ppm], p (MAA) adsorbent = 0.06 g for MG and 0.1 g for MB, room temperature).

Table 4: Pseudo second order kinetic parameters calculated from the linear outline for the adsorption of (a) MG and (b) MB from their various initial concentrations. The values of k_2 and q_e are represented in g/mg min^{-1} and mg g^{-1}, respectively (Reaction conditions; 100 ml solution of MG [60–360 ppm], MB [0–80 ppm], p (MAA) adsorbent = 0.06 g for MG and 0.1 g for MB, Room temperature).

Initial concentration	Constants	Malachite green (MG)	Methylene blue (MB)
MG = 60 ppm	k_2	0.003	0.044
MB = 20 ppm	q_e (calculated)	80.645	6.748
	q_e (experimental)	80.165	6.509
	R^2	0.999	0.996
MG = 120 ppm	k_2	0.005	0.029
MB = 30 ppm	q_e (calculated)	103.093	8.734
	q_e (experimental)	103.581	8.151
	R^2	0.999	0.983
MG = 240 ppm	k_2	0.0004	0.012
MB = 40 ppm	q_e (calculated)	294.118	19.763
	q_e (experimental)	288.403	19.130
	R^2	0.999	0.998
MG = 300 ppm	k_2	0.0001	0.005
MB = 50 ppm	q_e (calculated)	333.333	52.083
	q_e (experimental)	291.952	42.396
	R^2	0.994	0.996
MG = 360 ppm	k_2	0.0002	0.003
MB = 60 ppm	q_e (calculated)	370.370	54.347
	q_e (experimental)	351.774	52.493
	R^2	0.993	0.997
MB = 70 ppm	k_2	–	0.003
	q_e (calculated)	–	66.667
	q_e (experimental)	–	63.808
	R^2	–	0.997
MB = 80 ppm	k_2	–	0.002
	q_e (calculated)	–	73.529
	q_e (experimental)	–	70.255
	R^2	–	0.992

k_2= rate constants for pseudo second-order kinetcs, q_e = amount of adsorbate adsorbed per gram of the adsorbent at equilibrium condition, R^2 = coefficient of determination.

equilibrium adsorption. It was noted that the sorption rate was decreased as the sorption was developed from the first to third stage. This observation can be associated to the filling of binding sites gradually. In addition to the afore mentioned findings from IDP model, the straight lines of the three segments were not observed to pass through the origin. These findings propose that intraparticle diffusion played a part in the adsorption of MG and MB onto p (MAA) microgel, but it was not the only mechanism that affected the rate of adsorption.

Table 5: Parameters of intraparticle diffusion model calculated from the linear profiles for the adsorption of (a) MG and (b) MB from their different initial concentrations. The values of k_{id} and C are represented in (mg/g $min^{-0.5}$) and mg g^{-1}, respectively (Reaction conditions; 100 ml solution of MG [60–360 ppm], MB [20–80 ppm], p (MAA) adsorbent = 0.06 g for MG and 0.1 g for MB, Room temperature).

Initial concentration	Parameter	Malachite green (MG)	Methylene blue (MB)
MG = 60 ppm	k_{id}	6.653	0.890
MB = 20 ppm	C	23.590	2.494
	R^2	0.696	0.816
MG = 120 ppm	k_{id}	5.593	1.039
MB = 30 ppm	C	52.827	0.275
	R^2	0.466	0.777
MG = 240 ppm	k_{id}	23.166	1.659
MB = 40 ppm	C	59.732	4.139
	R^2	0.805	0.602
MG = 300 ppm	k_{id}	20.602	4.801
MB = 50 ppm	C	44.405	2.101
	R^2	0.921	0.786
MG = 360 ppm	k_{id}	31.587	4.385
MB = 60 ppm	C	39.503	11.104
	R^2	0.929	0.573
MB = 70 ppm	k_{id}	–	7.535
	C	–	10.451
	R^2	–	0.879
MB = 80 ppm	k_{id}	–	7.495
	C	–	8.264
	R^2	–	0.911

k_{id} = intraparticle diffusion rate constant, C = amount of adsorbate adsorbed per gram of adsorbent when t approaces to zero, R^2 = coefficient of determination.

The Elovich model proposes that as the concentration of adsorbate adsorbed on the surface of an adsorbent increases with an exponential decline in the rate of adsorption. This model also gives the information about the chemical adsorption and has been effectively used to describe the removal of solutes from a liquid solution, despite its origins in the kinetics of the adsorption of gases on solids. The mathematical expression of Elovich in the form of linear equation is demonstrated by Equation (8).

$$q_t = 1/\beta \ln (\alpha\beta) + 1/\beta \ln (t) \tag{8}$$

Here, α (mg/g min^{-1}) and β (g mg^{-1}) are the initial sorption rate, and desorption constant, respectively. Figure 10(a) and (b) depicts the graphical forms of linear equation of Elovich Model for MG and MB, respectively. The corresponding parameters are depicted in Table 6. Except for a couple of experiments, it was noted that with the rise in initial concentration the initial rate of adsorption was higher,

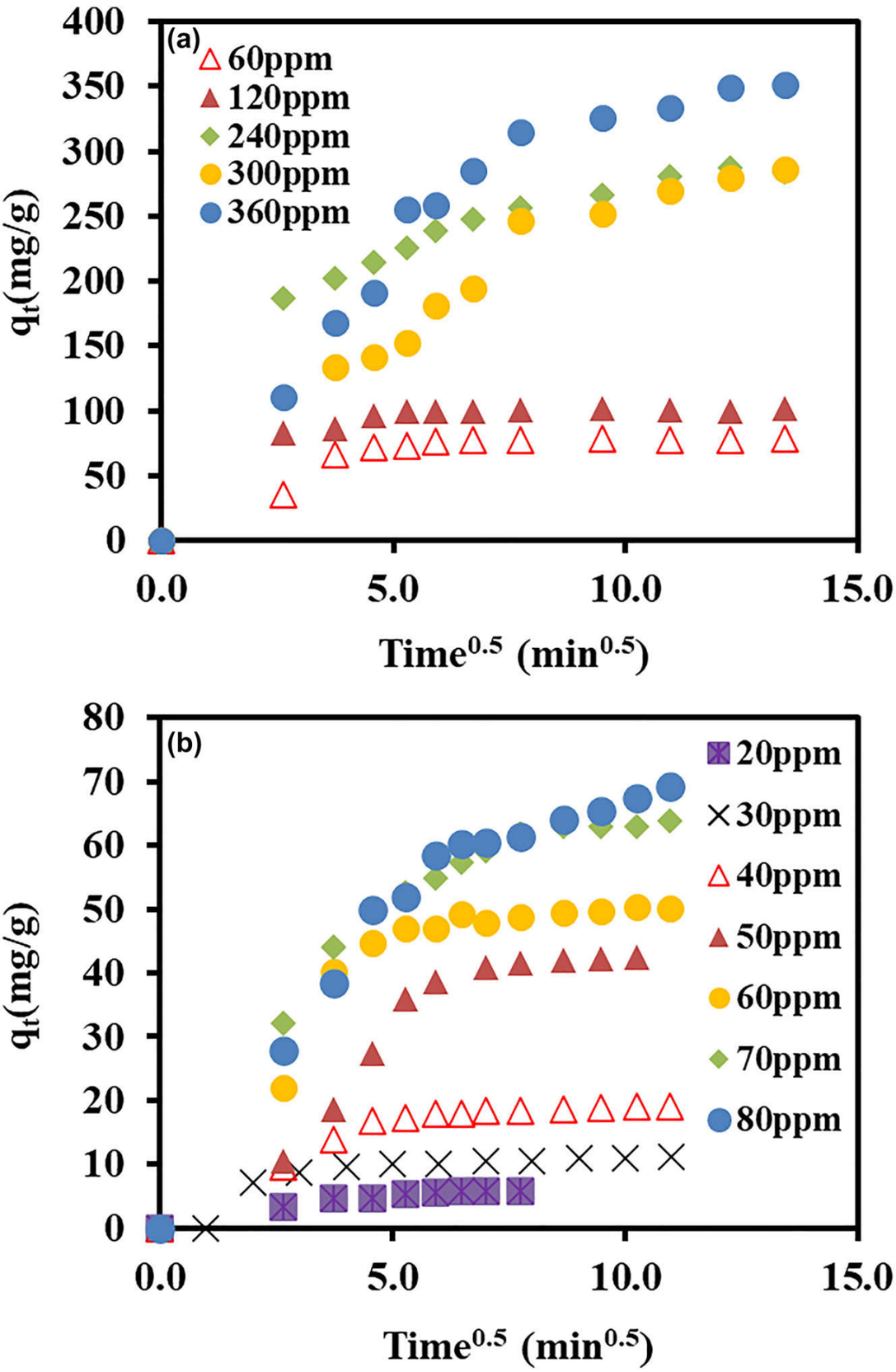

Figure 9: Plots of intraparticle diffusion model for the adsorption of (a) MG and (b) MB from their different initial concentrations (Reaction conditions; 100 ml solution of MG [60–360 ppm], MB [20–80 ppm], p (MAA) adsorbent = 0.06 g for MG and 0.1 g for MB, room temperature).

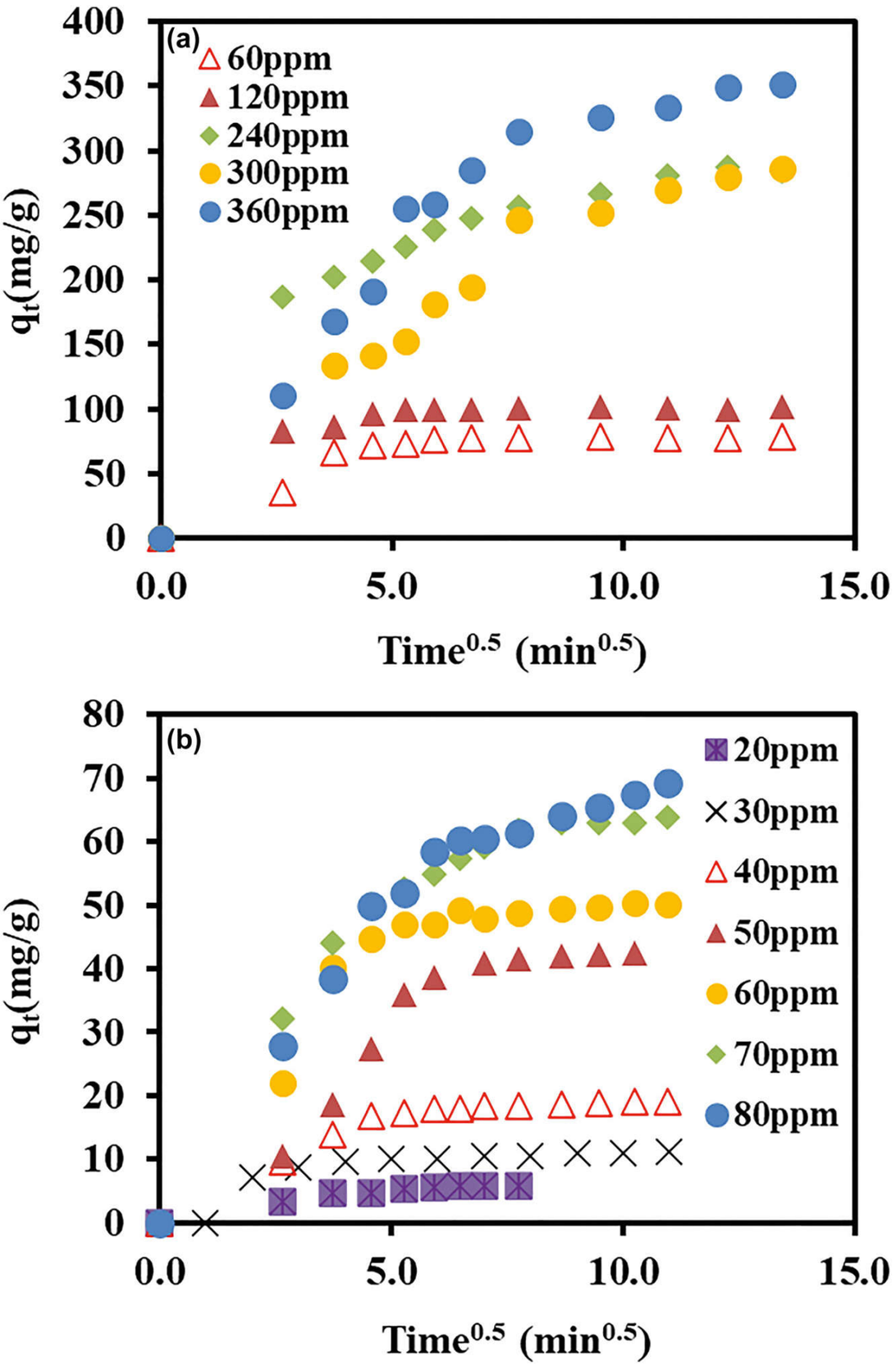

Figure 10: Plots of Elovich model for the adsorption of (a) MG and (b) MB from their different initial concentrations (Reaction conditions; 100 ml solution of MG [60–360 ppm], MB [20–80 ppm], p (MAA) adsorbent = 0.06 g for MG and 0.1 g for MB, room temperature).

Table 6: Parameters of Elovich model computed from the linear profiles for the adsorption of (a) MG and (b) MB from their different initial concentrations. The values of α and β are represented in mg g^{-1} min^{-1} and mg g^{-1} (Reaction conditions; 100 ml solution of MG [60–360 ppm], MB [20–80 ppm], p (MAA) adsorbent = 0.06 g for MG and 0.1 g for MB, Room temperature).

Initial concentration	Parameter	Malachite green (MG)	Methylene blue (MB)
MG = 60 ppm	α	46.487	1.893
MB = 20 ppm	β	0.073	0.713
	R^2	0.797	0.962
MG = 120 ppm	α	86.379	4.422
MB = 30 ppm	β	0.056	0.419
	R^2	0.747	0.924
MG = 240 ppm	α	22,127.480	7.033
MB = 40 ppm	β	0.002	0.252
	R^2	0.683	0.919
MG = 300 ppm	α	98.650	14.596
MB = 50 ppm	β	0.017	0.095
	R^2	0.959	0.931
MG = 360 ppm	α	71,423.85	15.797
MB = 60 ppm	β	0.001	0.091
	R^2	0.785	0.958
MB = 70 ppm	α	–	24.651
	β	–	0.081
	R^2	–	0.909
MB = 80 ppm	α	–	16.283
	β	–	0.068
	R^2	–	0.981

α = initial sorption rate, β = initial desorption constant, R^2 = coefficient of determination.

and desorption rate constant was decreased. These results indicate the chemical interactions between our investigated adsorbates and adsorbent.

4 Conclusions

The micron sized poly (methacrylic acid) microgel particles were prepared as anionic adsorbents and used successfully for the adsorptive removal of MG and MB. The adsorption capacity of the prepared poly (methacrylic acid) microgel was found as high as 351 mg g^{-1} and 65 mg g^{-1} for MG and MB, separately. The adsorption equilibrium was established in 60 min. The maximum removal percentage was recorded as 88 and 68% for MG and MB, respectively. By the application of adsorption isotherms, it was found that MG adsorption was best fitted with Langmuir model and that of MB was most suitable with Temkin model. It was discovered that the

adsorption data had a greater correlation with the pseudo second order kinetic model. The micron size of the p (MAA) microgel particles offered quick and easy adsorbent separation from the adsorption medium after the adsorption equilibrium. So, this work provides the idea of designing micron sized adsorbent particles for the fast adsorption equilibrium along with the advantages of their separation from the adsorption medium via a simple, quick, and easy process of filtration.

Acknowledgments: Financial support from Higher Education Commission (HEC), Pakistan under *Master leading to PhD, for the students of Aghaz-e-Haqooq-e-Balochistan Package* is highly acknowledged.
Author contribution: All the authors have accepted responsibility for the entire content of this submitted manuscript and approved submission.
Research funding: None declared.
Conflict of interest statement: The authors declare no conflicts of interest regarding this article.

References

1. Ma C., Zhou Z., Wei H., Yang Z., Wang Z., Zhang Y. *Nanoscale Res. Lett.* 2011, *6*, 1.
2. Roselin L. S., Selvin R. *Sci. Adv. Mater.* 2011, *3*, 113.
3. Ameen S., Seo H.-K., Akhtar M. S., Shin H. S. *Chem. Eng. J.* 2012, *210*, 220.
4. Laoufi N. A., Hout S., Tassalit D., Ounnar A., Djouadi A., Chekir N., Bentahar F. *Chem. Eng. Trans.* 2013, *32*, 1951.
5. Tan I., Ahmad A., Hameed B. *Desalination* 2008, *225*, 13.
6. Liu S., Ding Y., Li P., Diao K., Tan X., Lei F., Zhan Y., Li Q., Huang B., Huang Z. *Chem. Eng. J.* 2014, *248*, 135.
7. Foster F. J., Woodbury L. *Prog. Fish-Cult.* 1936, *3*, 7.
8. Stammati A., Nebbia C., De Angelis I., Albo A. G., Carletti M., Rebecchi C., Zampaglioni F., Dacasto M. *Toxicol. Vitro* 2005, *19*, 853.
9. Rodríguez-Herrera J., Cabado A. G., Bodelón G., Cunha S. C., Pinto V., Fernandes J. O., Lago J., Muñoz S., Pastoriza-Santos I., Sousa P. *Foods* 2021, *11*, 84.
10. Fallah A. A., Barani A. *Food Control* 2014, *40*, 100.
11. Omoregie E., Ofojekwu P., Anosike J., Adeleye A. *J. Aquacult. Trop.* 1998, *13*, 233.
12. Wright L. D. *Prog. Fish-Cult.* 1976, *38*, 155.
13. Srivastava S., Sinha R., Roy D. *Aquat. Toxicol.* 2004, *66*, 319.
14. Khan M. A., Otero M., Kazi M., Alqadami A. A., Wabaidur S. M., Siddiqui M. R., Alothman Z. A., Sumbul S. *J. Hazard Mater.* 2019, *365*, 759.
15. Hejtmancik M., Ryan M., Toft J., Persing R., Kurtz P., Chhabra R. *Toxicol. Sci.* 2002, *65*, 126.
16. Kanda M., Sridevi V., Pamu S. H., Bai M. T., Prasad K. N. *J. Environ. Treat. Tech.* 2022, *10*, 116.
17. Yan C., Dong J., Chen Y., Zhou W., Peng Y., Zhang Y., Wang L.-n. *Nano Res.* 2022, *15*, 3835.
18. Parshetti G., Kalme S., Saratale G., Govindwar S. *Acta Chim. Slov.* 2006, *53*, 492–498.
19. Gadow S. I., Estrada A. L., Li Y.-Y. *Bioresour. Technol.* 2022, *17*, 100886.
20. Mehandia S., Ahmad S., Sharma S., Arya S. K. *J. Water Proc. Eng.* 2022, *47*, 102662.
21. Mittal A. *J. Hazard Mater.* 2006, *133*, 196.

22. Abbasi E., Milani M., Fekri Aval S., Kouhi M., Akbarzadeh A., Tayefi Nasrabadi H., Nikasa P., Joo S. W., Hanifehpour Y., Nejati-Koshki K. *Crit. Rev. Microbiol.* 2016, *42*, 173.
23. Sayılkan F., Asiltürk M., Tatar P., Kiraz N., Arpac E., Sayılkan H. *J. Hazard Mater.* 2007, *148*, 735.
24. Krestou A., Xenidis A., Panias D. *Miner. Eng.* 2004, *17*, 373.
25. Crini G. *Bioresour. Technol.* 2006, *97*, 1061.
26. Sanghavi B. J., Wolfbeis O. S., Hirsch T., Swami N. S. *Microchim. Acta* 2015, *182*, 1.
27. Khani H., Rofouei M. K., Arab P., Gupta V. K., Vafaei Z. *J. Hazard Mater.* 2010, *183*, 402.
28. Köse T. E., Demiral H., Öztürk N. *Desalination Water Treat.* 2011, *29*, 110.
29. Janoš P., Buchtova H., Rýznarová M. *Water Res.* 2003, *37*, 4938.
30. Mckay G., Blair H., Gardner J. *J. Appl. Polym. Sci.* 1982, *27*, 3043.
31. Alpat S. K., Özbayrak Ö., Alpat Ş., Akçay H. *J. Hazard Mater.* 2008, *151*, 213.
32. Carrott P., Carrott M. R. *Carbon* 2009, *47*, 1012.
33. Oei B. C., Ibrahim S., Wang S., Ang H. M. *Bioresour. Technol.* 2009, *100*, 4292.
34. Gupta V. K., Jain R., Nayak A., Agarwal S., Shrivastava M. *Mater. Sci. Eng. C* 2011, *31*, 1062.
35. Bradder P., Ling S. K., Wang S., Liu S. *J. Chem. Eng. Data* 2011, *56*, 138.
36. Ali A. E.-H., Shawky H., Abd El Rehim H., Hegazy E. *Eur. Polym. J.* 2003, *39*, 2337.
37. DeMarco M. J., SenGupta A. K., Greenleaf J. E. *Water Res.* 2003, *37*, 164.
38. Cheng H., Scott K., Christensen P. *J. Appl. Electrochem.* 2005, *35*, 551.
39. Kaşgöz H., Özgümüş S., Orbay M. *Polymer* 2003, *44*, 1785.
40. Wu C.-H. *J. Hazard Mater.* 2007, *144*, 93.
41. Mittal H., Ray S. S. *Int. J. Biol. Macromol.* 2016, *88*, 66.
42. Cheng Z., Liao J., He B., Zhang F., Zhang F., Huang X., Zhou L. *ACS Sustain. Chem. Eng.* 2015, *3*, 1677.
43. Naseem K., Farooqi Z. H., Begum R., Ur Rehman M. Z., Ghufran M., Wu W., Najeeb J., Irfan A. *Environ. Sci. Pollut. Res.* 2020, *27*, 28169.
44. Shahid M., Farooqi Z. H., Begum R., Arif M., Irfan A., Azam M. *Chem. Phys. Lett.* 2020, *754*, 137645.
45. Farooqi Z. H., Sultana H., Begum R., Usman M., Ajmal M., Nisar J., Irfan A., Azam M. *Int. J. Environ. Anal. Chem.* 2022, *102*, 4104.
46. Hussain I., Shahid M., Ali F., Irfan A., Farooqi Z. H., Begum R. *Rev. Chem. Eng.* 2022; https://doi.org/10.1515/revce-2021-0075.
47. Rahman S., Al-Harbi F. F., Ajmal M., Naseem A., Farooqi Z. H., Siddiq M. *J. Mater. Sci.* 2022, *57*, 6763.
48. Mashkoor F., Nasar A. *J. Magn. Magn Mater.* 2020, *500*, 166408.
49. Ncibi M. C. *J. Hazard Mater.* 2008, *153*, 207.
50. Karimi S., Yaraki M. T., Karri R. R. *Renew. Sustain. Energy Rev.* 2019, *107*, 535.
51. Zayed A. M., Wahed M. S. A., Mohamed E. A., Sillanpää M. *Appl. Clay Sci.* 2018, *166*, 49.
52. Russo V., Trifuoggi M., Di Serio M., Tesser R. *Chem. Eng. Technol.* 2017, *40*, 799.
53. de Sá A., Abreu A. S., Moura I., Machado A. V. *Water Purification*; Elsevier: Cambridge, 2017; p. 289.
54. Sun L., Hu S., Sun H., Guo H., Zhu H., Liu M., Sun H. *RSC Adv.* 2015, *5*, 11837.
55. Fil B. A. *Part. Sci. Technol.* 2016, *34*, 118.
56. Hosseinzadeh H., Ramin S. *Int. J. Biol. Macromol.* 2018, *106*, 101.
57. Naseer F., Ajmal M., Bibi F., Farooqi Z. H., Siddiq M. *Polym. Compos.* 2018, *39*, 3187.
58. Umpuch C., Sopasin S. *ISTEC 2018 KEYNOTES*, 2018; p 53.